

## RESEARCH ARTICLE

10.1029/2018JD029435

# The Contributions of Winter Cloud Anomalies in 2011 to the Summer Sea-Ice Rebound in 2012 in the Antarctic

Yunhe Wang<sup>1,4,5</sup> , Xiaojun Yuan<sup>3</sup> , Haibo Bi<sup>1,2,5</sup>, Yu Liang<sup>1,4,5</sup> , Haijun Huang<sup>1,2,4,5</sup>, Zehua Zhang<sup>1,2,5</sup>, and Yanxia Liu<sup>1,2,5</sup>

<sup>1</sup>CAS Key Laboratory of Marine Geology and Environment, Institute of Oceanology, Chinese Academy of Sciences, Qingdao, China, <sup>2</sup>Laboratory for Marine Geology, Qingdao National Laboratory for Marine Science and Technology, Qingdao, China, <sup>3</sup>Lamont-Doherty Earth Observatory, Columbia University, New York, NY, USA, <sup>4</sup>University of Chinese Academy of Sciences, Beijing, China, <sup>5</sup>Center for Ocean Mega-Science, Chinese Academy of Sciences, Qingdao, China

## Key Points:

- Wintertime cloud fraction anomalies in 2011 contributed significantly to the summertime sea-ice rebound in 2012 in the Antarctic
- Less cloud fraction in winter 2011 related to large-scale atmospheric circulation resulted in a strong negative surface-radiation budget
- Cloud forcing in winter 2011 cooled the surface, promoted more sea-ice growth, and resulted in more sea-ice survival in summer 2012

## Correspondence to:

H. Bi and H. Huang,  
hbb@qdio.ac.cn;  
hjhuang@qdio.ac.cn

## Citation:

Wang, Y., Yuan, X., Bi, H., Liang, Y., Huang, H., Zhang, Z., & Liu, Y. (2019). The contributions of winter cloud anomalies in 2011 to the summer sea-ice rebound in 2012 in the Antarctic. *Journal of Geophysical Research: Atmospheres*, 124. <https://doi.org/10.1029/2018JD029435>

Received 2 AUG 2018

Accepted 21 FEB 2019

Accepted article online 1 MAR 2019

## Author Contributions:

**Funding acquisition:** Haibo Bi

**Methodology:** Haibo Bi

**Software:** Haibo Bi, Yu Liang

**Abstract** Unlike the rapid decline of Arctic sea ice in the warming climate, Antarctic sea-ice extent exhibits a modest positive trend in the period of near four decades. In recent years, the fluctuation in Antarctic sea ice has been strengthened, including a decrease toward the lowest sea-ice extent in February 2011 for the period of 1978–2016 and a strong rebound in the summer of 2012. The sea-ice recovery mainly occurs in the Weddell Sea, Bellingshausen Sea, Amundsen Sea, southern Ross Sea, and the eastern Somov Sea. This study offers a new mechanism for this summertime sea-ice rebound. We demonstrate that cloud-fraction anomalies in winter 2011 contributed to the positive Antarctic sea-ice anomaly in summer 2012. The results show that the negative cloud-fraction anomalies in winter 2011 related to the large-scale atmospheric circulation resulted in a substantial negative surface-radiation budget, which cooled the surface and promoted more sea-ice growth. The sea-ice growth anomalies due to the negative cloud forcing propagated by sea-ice motion vectors from September 2011 to January 2012. The distribution of the sea-ice anomalies corresponded well with the sea-ice concentration anomalies in February 2012 in the Weddell Sea and eastern Somov Sea. Thus, negative cloud-fraction anomalies in winter can play a vital role in the following summer sea-ice distribution.

## 1. Introduction

Contrasting to Arctic sea ice, which has decreased in all seasons and at nearly all locations (Comiso et al., 2017; Liu, Lin, Kong, et al., 2016; Liu, Lin, Wang, et al., 2016; Wang et al., 2018), the sea-ice extent (SIE) around Antarctica has displayed a marked seasonal cycle (Polvani & Smith, 2013) and a modest, but statistically significant, positive trend since 1979 (Hobbs et al., 2016; Holland, 2014; Simmonds, 2015). Also, different regional trend distributions exist in Antarctic sea-ice with rapid sea-ice loss in the Amundsen Sea and Bellingshausen Sea, while significant and moderate ice gain in the Ross Sea and Weddell Sea, respectively. Large cancellations from different sectors have resulted in a net positive trend in the Antarctic total SIE (Parkinson & Cavalieri, 2008).

However, the causes of the Antarctic sea-ice expansion remain a matter of debate, which could be caused by anthropogenic and natural factors. Some mechanisms have been suggested. Liu and Curry (2010) suggested that increased precipitation in the warming climate is an attributable factor for the current Antarctic sea-ice growth. In an ice-ocean modeling study, Zhang (2014) suggested that strengthened westerlies increase sea-ice volume by producing more ridged ice, which leads to sea ice more resilient to melting. There was a hypothesis that increased surface freshwater from the Antarctic continent and enhanced snowfall promote sea-ice expansion by stabilizing the upper water column (Rignot et al., 2013), which increases upper-ocean stratification and suppresses oceanic heat transport (Bintanja et al., 2013; Liu & Curry, 2010). In addition, the dipole pattern of the Pacific sector, combined with increasing sea ice in the Ross Sea and decreasing ice in the Bellingshausen Sea, has been ascribed to strengthening the Amundsen Sea low (Clem & Fogt, 2015; Fogt et al., 2012; Meehl et al., 2016; Raphael et al., 2016; Turner et al., 2016). Moreover, these sea-ice trend patterns around Antarctica have been attributed to interdecadal variability (Fan et al., 2014; Gagné et al., 2015), sea-surface temperature warming in the tropical Pacific (Clem & Fogt, 2015), and atmospheric intrinsic variability in the Antarctic (Turner et al., 2016).

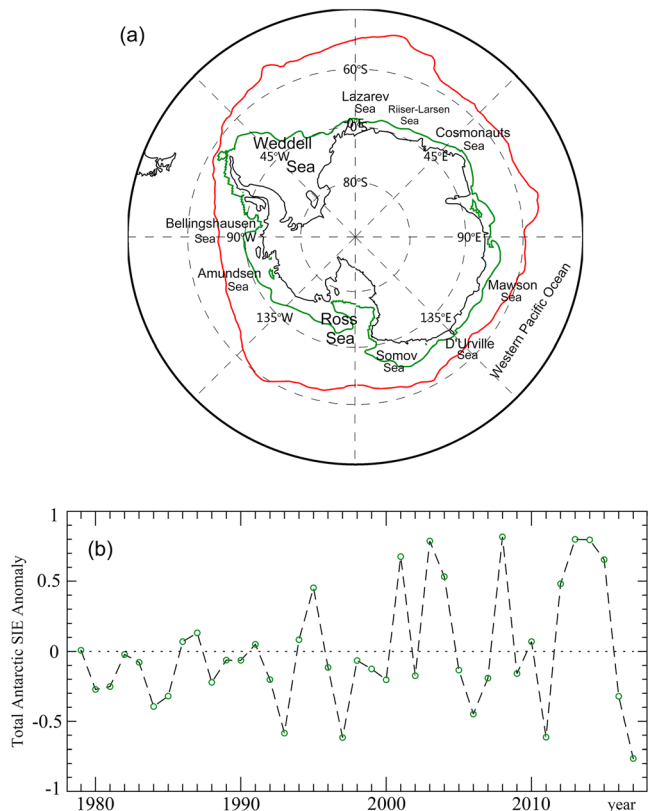


**Figure 1.** (a) Antarctic mean sea-ice edge in September (red line) and in February (green line) for the period of 2006–2015. Names of polar seas used in this study are marked. (b) Time series of the total Antarctic sea-ice extent (SIE) anomaly in February for the period of 1979–2017. The monthly sea-ice concentration used here is derived from the NASA Team algorithm and provided by the National Snow and Ice Data Center.

In addition to its rising trend, Antarctic SIE also shows significant inter-annual variability, especially in recent years. The Antarctic SIE in February 2011 hit the historical low for the period of 1978–2016, as depicted in Figure 1. Notably, the SIE in February 2012 ( $3.69 \times 10^6 \text{ km}^2$ ) represents a strong recovery from  $2.52 \times 10^6 \text{ km}^2$  (or a 46.4% SIE increase) in February 2011 (Figure 1). Sea ice restores its extent mainly over the Weddell Sea, Bellingshausen Sea, and the Amundsen Sea. It is also interesting to note that the decreases in sea-ice concentration (SIC) in the Bellingshausen Sea and Amundsen Sea were most significant during the last three decades (Cavalieri & Parkinson, 2008; Parkinson & Cavalieri, 2012). In this context, the cause of this strong short-term variability is worth discussing.

Previous studies suggested that cloud is capable of controlling the sea-ice growth and melting processes through its influences on the surface energy budget via reducing shortwave radiation and transmitting long-wave radiation (Huang et al., 2015; Lee et al., 2017; Liu et al., 2009; Liu & Key, 2014; Luo et al., 2017). Kapsch et al. (2013) argued that the years with negative SIC anomalies are associated with an increase in surface downwelling longwave radiation from increased cloud cover during spring. Some scientists agreed that cloud cover is an essential contributor to sea-ice variations (Cuzzone & Vavrus, 2011; Liu et al., 2012; Palm et al., 2010). Conversely, Schweiger et al. (2008) concluded that negative cloud anomalies combined with increased surface solar radiation in summer had no substantial contribution to the minimum SIE record. Nussbaumer and Pinker (2012) found that the accumulation of surface downwelling shortwave radiation did not correspond well to negative SIC anomalies.

Apparently, the large variations in SIE can mainly attribute to dynamic (wind stress and ocean currents) and thermodynamic factors (atmospheric temperature, ocean temperature, precipitation, etc.; Comiso & Nishio, 2008; Francis et al., 2009; Jacobs & Comiso, 1997; Liu & Curry, 2010; Manabe et al., 1991; Stammerjohn et al., 2012; Stroeve et al., 2012; Zhai et al., 2017; Zhang, 2008). The thermodynamic mechanism can alter the sea-ice thickness (SIT) through freeze-up or melting processes, and the dynamic mechanism is responsible for the redistribution of the SIT field. However, previous studies on the relationship among solar radiation, summertime cloud anomalies, and sea-ice anomalies have yielded inconsistent results (Graversen et al., 2011; Kapsch et al., 2013; Nussbaumer & Pinker, 2012). Therefore, the thermodynamic effects of clouds on sea-ice cover are not well understood in the Antarctic.

In this paper, we demonstrate that anomalous wintertime cloud cover could have a significant influence on the following summertime SIE in the Antarctic. We examined cloud forcing anomalies over the Southern Ocean in winter 2011 and their contributions to the SIE rebound in summer 2012 and quantified the effects on sea-ice growth via a sea-ice thermodynamic equation. The sea-ice motion data were used to calculate the cloud forced SIT anomaly redistribution from September 2011 to January 2012. It helps to assess how wintertime cloud forcing anomalies contributed to the significant return of ice cover in February 2012.

## 2. Data

The monthly mean SIC derived by the NASA Team algorithm with a grid cell size of  $25 \times 25 \text{ km}$  is obtained from the National Snow and Ice Data Center (NSIDC). This data set is retrieved from multiple satellite measurements, including the Scanning Multichannel Microwave Radiometer on the Nimbus-7 satellite, the Defense Meteorological Satellite Program Special Sensor Microwave/Imager on the F8, F11, and F13 satellites, and the Special Sensor Microwave Imager/Sounder aboard the Defense Meteorological Satellite Program F17 satellite (Parkinson & Cavalieri, 2012). Daily gridded sea-ice motion vectors, which are obtained from the NSIDC and projected onto the 25-km Southern Hemisphere Equal-Area Scalable Earth

Grids, are derived from the Advanced Very High Resolution Radiometer, Special Sensor Microwave/Imager, Scanning Multichannel Microwave Radiometer, and International Arctic Buoy Program buoy data. The grid field extends from 53.2°S to 90°S for the entire time series.

The Modern-Era Retrospective analysis for Research and Applications (MERRA) reanalysis is utilized here, which uses the Goddard Earth Observing System version 5 data assimilation system. It is a U.S. NASA reanalysis data set during the satellite era from 1979 to today (Zhang et al., 2018). The native MERRA grid has a spatial resolution of 0.5° latitude by 0.67° longitude, with 72 hybrid-model levels in the vertical (Bosilovich et al., 2011). The European Centre for Medium-Range Weather Forecasts (ECMWF) Interim Reanalysis (ERA-Interim) is also used primarily for comparison. The ERA-Interim reanalysis is the latest global atmospheric reanalysis produced by the ECMWF and covers the period 1979 to present (Dee et al., 2011). It includes improvements from the earlier data set with more extensive assimilation of satellite radiances, improved model physics, and an assimilated model with higher spectral resolution and provides a 12-hr four-dimensional data assimilation (Screen & Simmonds, 2012; Svensson & Karlsson, 2011). These reanalysis products all include cloud fraction, the surface net downward shortwave and longwave fluxes under all and clear sky, geopotential height, specific humidity, air temperature, wind, and vertical pressure velocity at 850 hPa. In this paper, we used total cloud fraction as the metric, which begins at 1,000 hPa and up in the MERRA. The height of cloud top could vary in the Goddard Earth Observing System version 5. Different cloud top heights may affect the long wave characteristics.

Besides these reanalysis data sets, we also examine satellite observations of cloud cover. The Advanced Very High Resolution Radiometer Polar Pathfinder—Extended (APP-x) product (Key, 2016; Wang & Key, 2003, 2005a, 2005b) contains cloud fraction, which is retrieved at high and low sun times (14:00 and 02:00 local solar time for the Antarctic) using a radiative transfer model and a suite of algorithms (Katlén et al., 2017). The APP-x cloud record on a 25-km Equal-Area Scalable Earth Grid begins in 1982 and continues to the present. The International Satellite Cloud Climatology Project (ISCCP) data set of cloud fraction has a more than 30-year archive of daily global observations. The ISCCP data set utilizes radiance information from a series of geostationary satellites to create three-hourly maps of cloudiness and other associated products. The ISCCP-H monthly mean cloud product with a resolution of 8 km at nadir for the period of 2006–2014 was used here.

The SIT can be estimated by a thermodynamic model with optical (visible, near-infrared, and infrared) provided by APP-x observations (Wang et al., 2010). These satellite data provide an opportunity to investigate the SIT over the entire Antarctic region with high spatial and temporal resolutions.

### 3. Cloud-Fraction Anomaly

Unless noted otherwise, all anomalies reported in this paper are larger than two standard deviations of the monthly mean from 2006 to 2015. The cloud fraction in July 2011 obtained from the MERRA reanalysis shows strong negative anomalies mostly over the Weddell Sea, Indian Ocean, western Pacific Ocean, Bellingshausen Sea, and the Amundsen Sea (Figure 2a). The cloud anomalies were approximately  $-20\%$  below the normal over the Weddell Sea and Bellingshausen Sea. The negative cloud anomalies in 2011 winter were substantial and had a potential radiative impact on sea-ice growth. Moreover, this negative anomaly is not transient. However, cloud-fraction anomalies in January 2012 (shown in Figures 2b and 2d), December 2011, and February 2012 (not shown) were neither significant nor widespread. Lack of strongly negative cloud anomalies suggests that sea-ice rebound in summer 2012 cannot be directly related to summer cloud forcing, which is consistent with previous works (Kauker et al., 2009; Schweiger et al., 2008). These early studies could not find what links cloud-cover anomalies in summer to the minimum SIE.

ERA-Interim reanalysis (Figure 2c) and satellite measurements of APP-x (Figure 2e) and ISCCP (Figure 2f) present the consistent cloud anomaly distribution in July 2011 as those of the MERRA. The anomaly is computed relative to the mean for the period 2006–2014 for the ISCCP because of the limited time series and for the period 2006–2015 for other data. They all show negative anomalies over the Weddell Sea, Bellingshausen Sea, Amundsen Sea, and the western Pacific Ocean, although some differences exist among these data sets. For example, negative cloud cover anomalies in the Weddell Sea, Amundsen Sea, and the Bellingshausen Sea from APP-x and MERRA are more extensive than that from ISCCP. Besides, the positive cloud cover anomalies over the Ross Sea in APP-x are more widespread compared to that of MERRA and ISCCP.

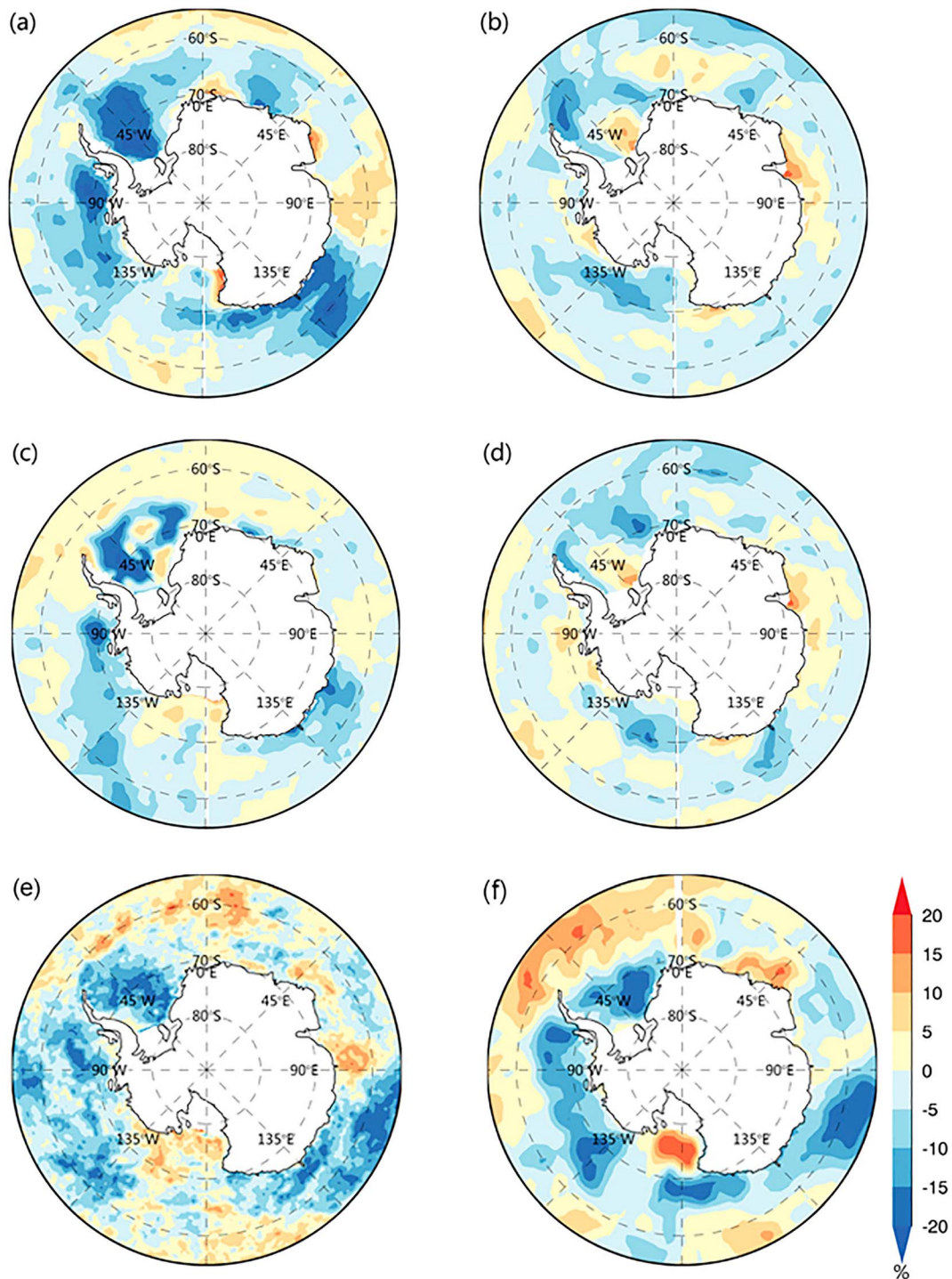


**Figure 2.** Antarctic cloud fraction anomalies (unit: %) in (a) July 2011 and (b) January 2012 from the Modern-Era Retrospective analysis for Research and Applications reanalysis, in (c) July 2011 and (d) January 2012 from the ERA-Interim reanalysis, and in July 2011 from the Advanced Very High Resolution Radiometer Polar Pathfinder—Extended satellite data (e) and the International Satellite Cloud Climatology Project (ISCCP) data (f). The anomaly is computed relative to the mean for the period 2006–2014 for the ISCCP because of the limited time series and for the period 2006–2015 for other data.

Dolinar et al. (2016) argue that the MERRA reanalysis underpredicts the global (45°N/S) mean cloud fraction by 2.7% for the period March 2000 to February 2012, comparing to satellite observations (Moderate Resolution Imaging Spectroradiometer). Nevertheless, the anomaly patterns and magnitudes from MERRA, ERA-Interim, APP-x, and ISCCP are similar in most polar seas around Antarctica.

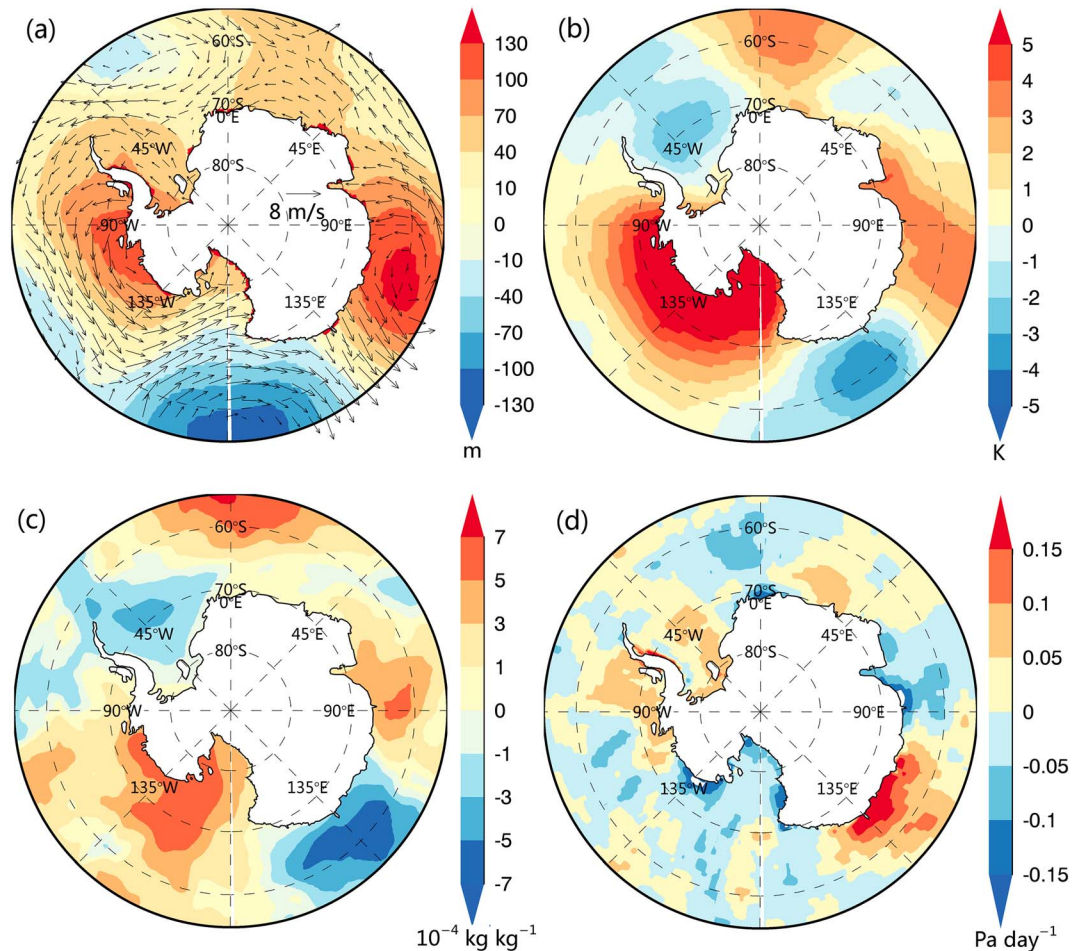


**Figure 3.** The 850-hPa (a) geopotential height anomalies (unit: m), wind anomalies (unit: m/s), (b) air temperature anomalies (unit: K), (c) specific humidity anomalies (unit:  $10^{-4}$  kg/kg), and (d) vertical pressure velocity anomalies (unit: Pa/day) from the Modern-Era Retrospective analysis for Research and Applications reanalysis for July 2011.

Therefore, the similarity among these data sets supports that a robust less cloud event occurred in 2011 winter.

To understand what caused the less cloud cover, we examined the atmospheric circulation in winter 2011. In July 2011, the geopotential height at 850 hPa had a strong negative anomaly centered at  $180^{\circ}\text{E}$  and two positive anomaly centers in the Mawson Sea and Bellingshausen/Amundsen Seas, respectively (Figure 3a). The geostrophic wind associated with this pressure pattern transported cold and dry air from Antarctica to polar seas, creating low temperature and low humidity in the Weddell Sea and D'Urville Sea (Figure 3b and 3c). Negative cloud-fraction anomalies correspond well with descending air (positive vertical pressure velocity in Figure 3d) in the western Weddell Sea, Bellingshausen Sea, D'Urville Sea, and the Riiser-Larsen Sea. It appears that the advection of cold/dry air from Antarctica creates low temperature and low humidity condition, prohibiting cloud formation. The less cloud coverage allows more heat escape and further cools the surface, which could lead to more downward vertical motion. This positive feedback process could generate widespread negative cloud anomalies, frigid winter, and more sea-ice production in winter 2011.

In August 2011, the MERRA reanalysis also showed negative cloud-cover anomalies in most polar seas around Antarctica (Figure 4b). Anomalous pressure propagated eastward, but its quadrature phase-shifted relationship with cloud anomaly distribution remains the same (Figures 4a and 4b). In response to the anomalous geopotential height, the cloud-fraction anomaly became more apparent over the Antarctic Peninsula, Drake Passage, eastern Weddell Sea, Cosmonauts Sea, and the northern D'Urville Sea. Also, it is worth noting that the most significant negative cloud anomaly from the MERRA reanalysis was over

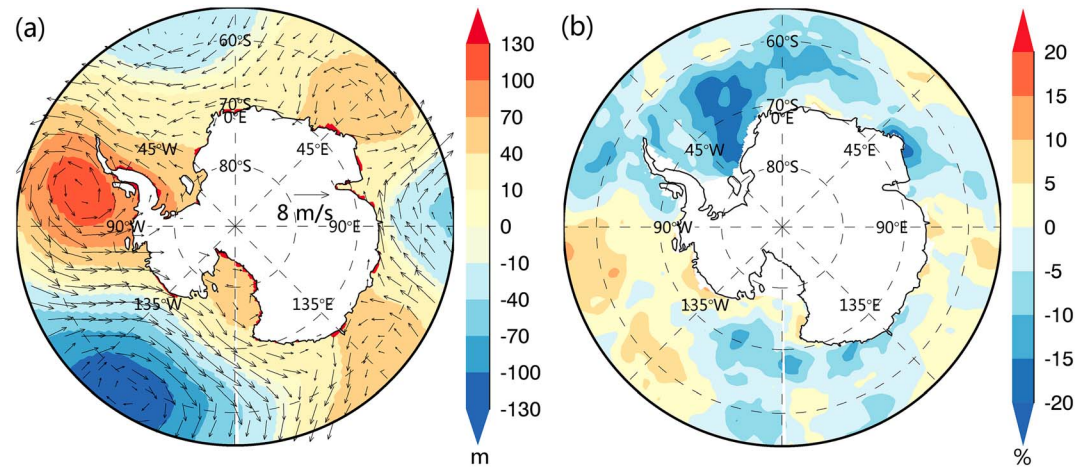


**Figure 4.** The 850-hPa geopotential height anomalies (unit: m) and wind anomalies (unit: m/s; a) and the cloud fraction anomalies (unit: %; b) from the Modern-Era Retrospective analysis for Research and Applications reanalysis for August 2011.

the eastern Lazarev Sea, where the cold advection by the geostrophic winds was not significant. Thus, it is suggested that large-scale atmospheric circulation may not be a single cause of cloud amount anomalies in the Antarctic.

#### 4. Cloud Forcing Anomaly at the Surface

Cloud forcing, or the cloud radiative effect, is the net radiation flux difference between average cloud conditions and average cloud-free conditions. Surface cloud forcing comprises shortwave and longwave cloud radiative forcing at the surface. On the one hand, clouds shelter the shortwave radiation budget mainly via their high albedo. On the other hand, they influence on longwave radiation budget by changing the emitting temperature and atmospheric emissivity. Therefore, clouds have a cooling effect on the surface for solar radiation but a warming effect in terms of longwave radiation. Overall, the impact of clouds on the surface radiation budget depends on the balance between surface shortwave and longwave radiation budgets associated with clouds. Surface cloud forcing is the integration of partial derivative of the radiation flux associated with cloud amount and is calculated from net shortwave and longwave radiative fluxes at the surface. It is defined by Wang and Key (2005a) as

$$CF_{\lambda,z} = \int_0^{A_c} \frac{\partial F_{\lambda,z}}{\partial \alpha} da = F_{\lambda,z}(A_c) - F_{\lambda,z}(0) \quad (1)$$

$$CF_z = CF_s + CF_l \quad (2)$$

where  $CF_{\lambda,z}$  represents the shortwave or longwave cloud forcing at the surface,  $F_{\lambda,z}$  represents the surface net flux in shortwave or longwave radiation,  $\lambda$  represents the wavelength,  $z$  represents the altitude above the surface, and  $A_c$  represents cloud fraction.  $CF_z$  represents all-wave cloud forcing, and  $CF_s$  and  $CF_l$  represent shortwave and longwave cloud forcing at the surface, respectively.

Due to the absence of solar radiation, Antarctic cloud forcing is dominated by longwave cloud forcing in winter. The cloud shortwave radiative effect is mainly distributed north of 66.5°S. Surface cloud forcing derived from the MERRA reanalysis shows negative anomalies over most of the Southern Ocean around Antarctica in winter (Figure 5). The cloud forcing anomaly is approximately  $-20 \text{ W/m}^2$  over the Weddell Sea,  $-15 \text{ W/m}^2$  over the Somov Sea,  $-10 \text{ W/m}^2$  over the Ross Sea, and  $-8 \text{ W/m}^2$  over the D'Urville Sea and Bellingshausen Sea. The net radiative flux anomaly patterns are controlled by cloud cover over the Weddell Sea, D'Urville Sea, and the northern Lazarev Sea in winter 2011. However, these anomaly patterns do not correspond well to the cloud-fraction anomalies over the Ross Sea, Bellingshausen Sea, and the Amundsen Sea, where positive net radiative flux anomalies of approximately  $8 \text{ W/m}^2$  occur. This result indicates that the net radiative flux anomalies are partially influenced by cloud cover in winter over the Southern

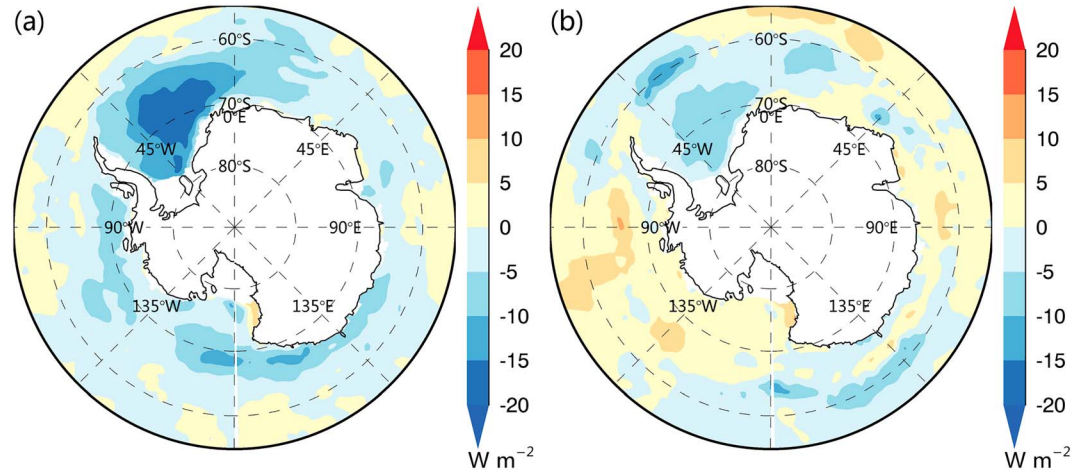


**Figure 5.** Surface cloud forcing anomalies (a) and net radiative flux anomalies (b) in winter (defined as June, July, and August) from the Modern-Era Retrospective analysis for Research and Applications reanalysis (unit:  $\text{W}/\text{m}^2$ ). The surface cloud forcing anomaly is calculated by shortwave and longwave cloud forcing anomalies at the surface. The surface net radiative flux anomaly is computed via the surface net shortwave and longwave radiative flux anomalies.

Ocean around Antarctica, and they are also affected by other atmospheric components, such as water vapor, aerosols, carbon dioxide, and ozone, which are not the focus of this paper (Jing & Lin, 2017; Lin et al., 2016; Mei et al., 2012; Sun et al., 2015; Wang et al., 2017; Wu et al., 2017). The cloud-cover anomalies resulted in strong negative cloud forcing in winter 2011, which interrupted the surface energy balance and had an important influence on the sea-ice growth.

### 5. Contributions of Cloud Forcing Anomalies on Sea Ice in Summer

Negative anomalies in surface cloud forcing favor sea-ice growth. Here we present the calculations for the thermodynamic effects of climatic indices on sea-ice via the sea-ice growth model (Maykut et al., 1992; Parkinson & Washington, 1979). The expression for sea-ice growth is

$$-\Delta h = \frac{\Delta t}{\rho L} [H_{\downarrow} + LE_{\downarrow} + \epsilon_w LW_{\downarrow} + (1 - \alpha_w) SW_{\downarrow} + F_{I\uparrow} + F_{w\uparrow}] \quad (3)$$

where  $\Delta h$  represents sea-ice growth,  $\Delta t$  represents the time step,  $\rho$  represents the density of sea ice ( $917 \text{ kg}/\text{m}^3$ ),  $L$  represents the latent heat of fusion for sea ice ( $333.4 \text{ kJ}/\text{kg}$ ),  $H_{\downarrow}$  represents sensible heat,  $LE_{\downarrow}$  represents latent heat,  $LW_{\downarrow}$  represents incoming longwave radiation with  $\epsilon_w$  longwave emissivity,  $SW_{\downarrow}$  represents incoming shortwave radiation with the surface albedo ( $\alpha_w$ ) depending on the surface characteristics,  $F_{I\uparrow}$  represents the heat flux emitted from the surface, and  $F_{w\uparrow}$  represents the conductive heat flux at the ice-ocean interface. However, the focus of this study is the effect of surface cloud forcing on sea ice, and the other factors in the equation, including  $H_{\downarrow}$ ,  $LE_{\downarrow}$ ,  $F_{I\uparrow}$ , and  $F_{w\uparrow}$ , are much smaller than the radiative fluxes. Thus, we simplified the equation by neglecting these small factors and combining these specified variables as follows:

$$-\Delta h = \frac{\Delta t}{\rho L} [FL_{w\downarrow} + FS_{w\downarrow}] \quad (4)$$

where  $FL_{w\downarrow}$  and  $FS_{w\downarrow}$  represent the surface net fluxes of longwave and shortwave radiation, respectively. This equation is similar to equation (1) in Eisenman et al. (2007). To facilitate the statistical calculation, we need to separate cloud forcing from the surface radiative fluxes, as shown below:

$$-\Delta h = \frac{\Delta t}{\rho L} [CF_z + F_{\text{net}}(0)] \quad (5)$$

where  $F_{\text{net}}(0)$  represents the surface net radiative flux for clear sky and can be calculated by adding the surface net shortwave and longwave radiative fluxes under clear-sky.  $CF_z$  represents the surface net cloud

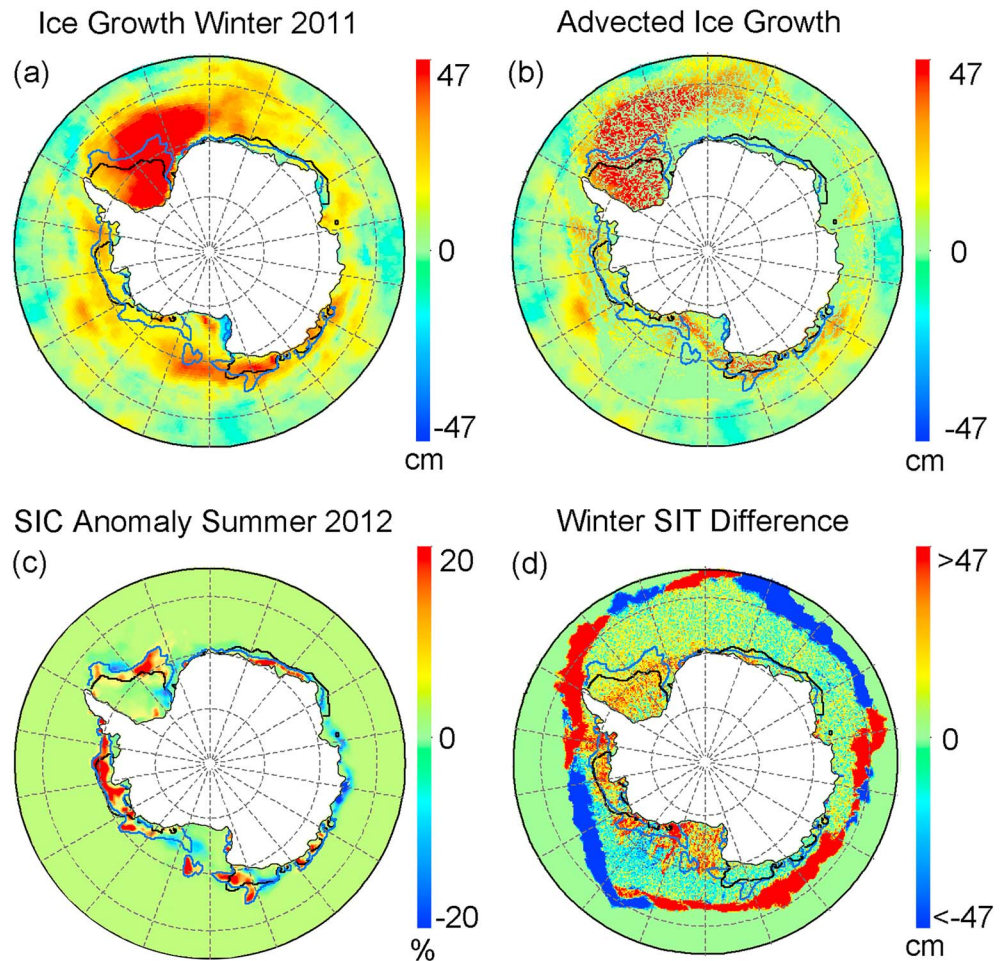


**Figure 6.** (a) Sea-ice growth estimated by surface cloud forcing anomalies during winter (June–August) 2011 from the Modern-Era Retrospective analysis for Research and Applications reanalysis (unit: cm). The land area is marked with white, the blue lines represent the sea-ice extent (SIE) in February 2012, and the black lines represent the SIE in February 2011. (b) Sea-ice thickness (SIT) anomaly distribution modified by the sea-ice motion from September 2011 to January 2012. (c) Sea-ice concentration (SIC) anomalies in February 2012 from the monthly mean SIC product used in the NASA Team algorithm (unit: %). (d) The difference in SIT between September 2011 and September 2010 based on the Advanced Very High Resolution Radiometer Polar Pathfinder—Extended satellite data.

forcing and can be calculated by adding the surface net shortwave and longwave cloud forcing. Thus, we estimate ice growth under the cloud forcing via equation (6).

$$-\Delta h = \frac{\Delta t}{\rho L} CF_z \quad (6)$$

This assumption has some limitations. For example, the turbulent fluxes play a vital role over the polynyas, which are a common feature of the circumpolar Antarctic sea ice zone (Tamura et al., 2016). Most Antarctic polynyas occur adjacent to the coastline and on the narrow continental shelf (Tamura et al., 2008). They can boost the sea-ice formation rate by the intensive heat lost from the ocean to the atmosphere during winter. However, the areas of polynyas are very small comparing to the total winter sea-ice area (Tamura et al., 2016). So the overall turbulent fluxes from polynyas are insignificant when averaged over the whole Antarctic sea ice cover in winter.

Applying equation (6), a  $1\text{-W/m}^2$  anomaly in the negative net cloud forcing at the surface in winter (June to August) would generate approximately 2.60 cm of sea ice. Based on the results calculated by equation (6), sea-ice growth anomalies due to cloud forcing are mostly positive, particularly large in the Weddell Sea and Ross Sea during the winter 2011 (Figure 6a). Focusing on summer sea-ice anomaly, we calculated the

**Table 1***Regional Mean Sea-Ice Growth in Winter 2011 and the Drifted Mean Ice Accumulation at the Beginning of February 2012 (Unit: cm)*

SIT	Weddell Sea (60°W, 20°W)	Indian Ocean (20°W, 90°E)	D'Urville Sea (110°E, 140°E)	Somov Sea (140°E, 180°)	Ross Sea (180°, 140°W)	Amundsen Sea (140°W, 100°W)	Bellingshausen (100°W, 60°W)
SIT in winter 2011	30.2	4.6	17.0	20.1	10.8	8.7	14.9
SIT in Feb. 2012	17.1	0.1	4.1	10.2	7.5	5.7	7.0

Note. The sea-ice growth was calculated only inside the February 2012 sea-ice extent boundary lines. SIT = sea-ice thickness.

regional mean sea-ice growths in winter 2011 inside the SIE boundary lines for February 2012 (Table 1). The results show that it generated 30.2 cm sea ice over the Weddell Sea, 20.1 cm over the Somov Sea, 17.0 cm over the D'Urville Sea, 14.9 cm over the Bellingshausen Sea, and 10.8 cm over the Ross Sea. The anomalous patterns in sea-ice growth in winter 2011 are very similar to the distributions of SIC anomalies in February 2012, where positive anomalies are mainly in the Southern Ocean around western Antarctica (Figure 6c). Specifically, the increased sea-ice growth corresponds to the positive SIC anomalies in the Weddell Sea, Bellingshausen Sea, Amundsen Sea, northern Ross Sea, and the eastern Somov Sea.

Note that the anomalies in winter sea-ice growth and summer SIC in Figure 6 do not match in some areas. For example, the 2012 summer SIC anomalies are negative in the Lazarev Sea and Indian Ocean (Figure 6c), while the cloud forced winter sea-ice growth anomalies are positive there (Figure 6a). This discrepancy can be partially explained by ice drift. As pointed out by Holland and Kwok (2012), the changes in the sea-ice cover are closely related to ice drift around Antarctica. Early model studies show that ice motion can induce changes in the SIT and SIC spatial distribution (Holland et al., 2014; Massonnet et al., 2013).

To examine where winter cloud forced sea-ice anomaly goes, we calculated its movement using sea-ice motion vectors from the beginning of September 2011 to the end of January 2012. Figure 6b shows the redistribution of the winter cloud forced sea-ice anomaly by ice motion at the end of January. Apparently, the cloud forced sea-ice growth anomalies in the Lazarev Sea and Indian Ocean were moved by ice drift, which are consistent with the negative summer SIE. Besides, the positive winter sea-ice growth anomalies in the eastern Ross Sea were also removed by ice drift, which does not contribute to the positive sea-ice anomalies there in summer 2012. Thus, other processes, such as freshwater influx, ocean heating, and large-scale atmospheric circulation, may be the influencing factors to sea-ice summer distribution in the area. To quantitatively reflect the contribution of winter cloud anomalies to following summer sea ice, we calculated the mean regional surviving SIT from Figure 6b only inside the February 2012 sea-ice edge (blue), as shown in Table 1. The surviving cloud forced SIT anomaly is substantial over the Weddell Sea (17.05 cm) and eastern Somov Sea (10.15 cm), which corresponded to an anomalously high SIE over these regions in February 2012 (Figure 6c).

Figure 6d shows that SIT in the winter of 2011 is greater than that in winter 2010 over the southern Weddell Sea, southern Bellingshausen Sea, southern Amundsen Sea, and the northern Somov Sea, where negative cloud-forcing anomalies occurred in winter 2011. This consistency provides direct evidence that winter cloud-cover anomalies produced excessive thicker sea ice in winter 2011. This thicker winter sea-ice anomaly likely persisted through the following seasons in these areas and resulted in positive SIC anomaly in summer 2012.

## 6. Discussion and Conclusions

We demonstrate that anomalous wintertime cloud cover could have a significant influence on the following summertime SIE in the Antarctic. The results reveal that the cloud-cover anomalies corresponded well with the cold and warm advection by the geostrophic winds associated with the pressure pattern and vertical air motion, suggesting that an anomalous pressure system was likely a cause for negative cloud anomalies in winter 2011. Furthermore, the cloud amount anomaly led to stronger negative cloud forcing, which cooled the surface and allowed for greater ice growth in the abnormal cloud amount regions. Sea-ice growth that resulted from cloud forcing in the winter 2011 was analytically estimated to be as much as 30.2 cm in the Weddell Sea, 20.1 cm in the Somov Sea, 10.8 cm in the Ross Sea, 17.0 cm in the D'Urville Sea, and 14.9 cm in the Bellingshausen Sea. After applying the ice-motion field from September 2011 to January

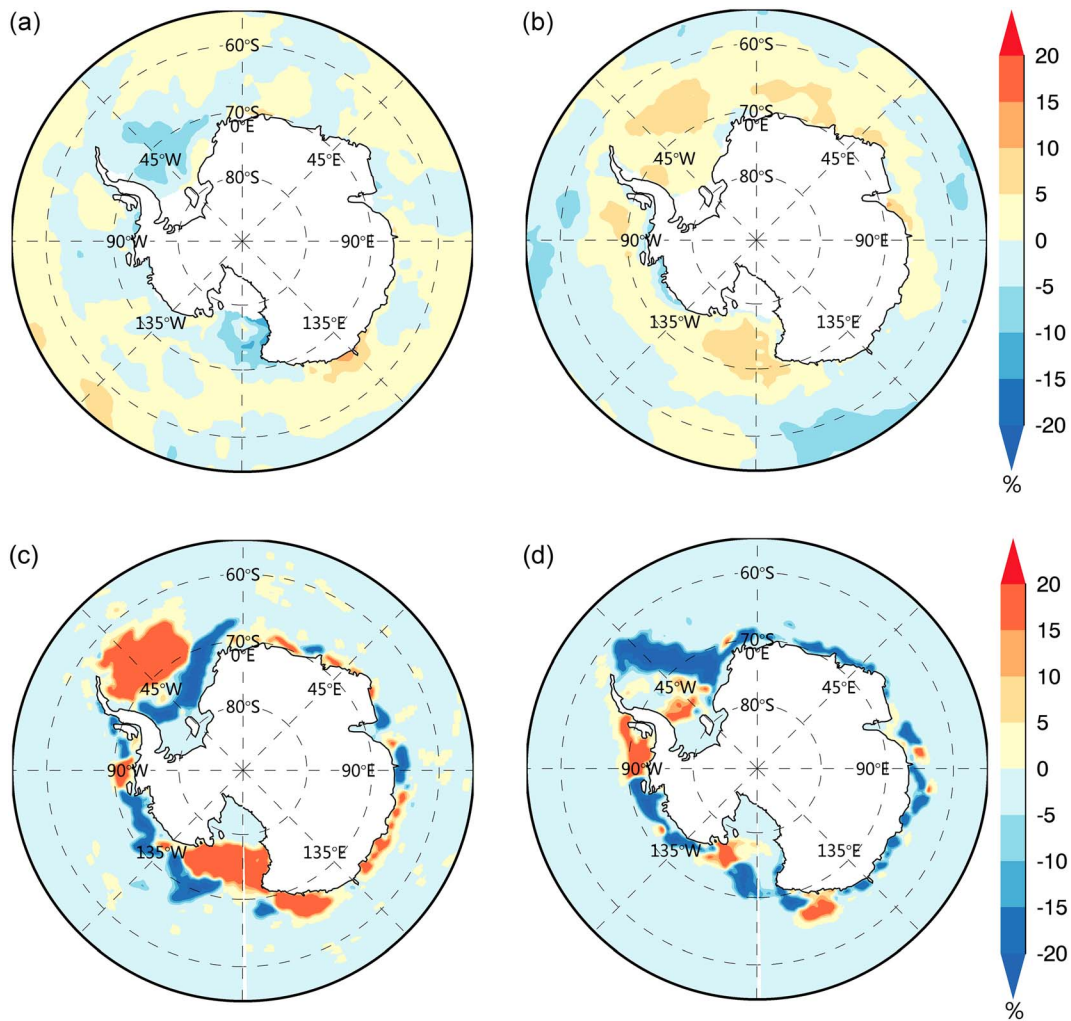


**Figure 7.** Antarctic cloud fraction anomalies in the winter (June–August) of 2002 (a) and 2015 (b) from the Modern-Era Retrospective analysis for Research and Applications reanalysis. Antarctic sea-ice concentration differences (unit: %) between February 2003 and February 2002 (c) and between February 2016 and February 2015 (d). The anomaly in the winter of 2002 is computed relative to the mean for the period 1997–2006, and the anomaly in the winter of 2015 is computed relative to the mean for the period 2006–2015.

2012, the distribution of winter cloud forced sea-ice growth corresponded well with February 2012 SIC anomalies over the Weddell Sea and eastern Somov Sea. Also, the areas with enhanced SIT in September 2011 relative to the SIT in September 2010, again coincide with the areas of anomalous negative cloud forcing in the winter of 2011. Thus, less cloud cover in the winter of 2011 played a vital role in the return of Antarctic sea ice in summer 2012. The absence of significant summertime cloud anomalies suggests that the summertime clouds had a minor effect on the sea-ice rebound in 2012.

However, the anomalies in winter sea-ice growth and summer SIE in Figure 6b do not match in some sea. For example, the positive sea-ice growth anomalies in the eastern Ross sea were moved by ice drift, which does not explain the positive sea-ice anomalies in summer 2012 there, because many other factors may affect sea-ice growth, such as ocean currents, wind, and even water vapor, aerosols, and carbon dioxide (Rosenfeld et al., 2014; Zhang, 2014). Moreover, the distinct high-latitude climate modes, such as the quasistationary wave-3 pattern, semiannual oscillation, Southern Annular Mode (SAM), and Pacific South American pattern, exist in the Southern Hemisphere at intraseasonal to decadal timescales (Pezza et al., 2012; Yuan & Li, 2008; Yuan & Martinson, 2001; Yuan & Yonekura, 2011). Lefebvre et al. (2004) concluded that SIC response to SAM is out-of-phase in the Ross Sea and Weddell Sea instead of a zonally symmetric response. Pezza et al. (2012) argue that the correlations of SIE and SAM are negative in the Bellingshausen/west

Weddell. Figure 6 reflected that the sea-ice rebound in summer 2012 is mainly attributed to the sea ice increasing in the Weddell Sea, Bellingshausen Sea, and the Ross Sea. The SAM index varies from the negative phase to positive during the period of March 2011 to February 2012 with the mean 0.25. Thus, the overall weak positive SAM unlikely contributes to the sea-ice recovery in February 2012.

Furthermore, the impacts of winter cloud forcing on sea ice can only be traced in the following summer ice field in a few regions around Antarctica where summer sea ice can survive. The Weddell Sea and Ross Sea are among these regions (Cavalieri & Parkinson, 2008). In the eastern Antarctic, sea ice usually completely melts in summer (Figure 1a); therefore, it is difficult to detect the residual anomalies from winter. In winter 2011, negative cloud anomalies were primarily distributed in the Weddell Sea, Bellingshausen Sea, Amundsen Sea, Ross Sea, and the Southwestern Pacific, which allowed the cloud effect on sea ice to be retrained through the following summer. The spatial distribution of negative cloud anomalies in winter 2011 is also a factor that the 2012 summer sea-ice anomaly can be traced back to winter cloud forcing.

In this study, we show that the winter cloud anomalies in 2011 can affect the sea-ice distribution in the following summer. Such an event did not only occur in winter 2011 to summer 2012. Similarly, the less cloud-fraction in the winter of 2002 preceded the more sea ice in the summer of 2003 (Figures 7a and 7c). On the contrary, the positive cloud-fraction anomalies in winter 2015 enhanced long-wave radiation and reduced sea-ice growth, which likely to contribute to the ice retreat in summer 2016 (Figures 7b and 7d).

The impact of winter cloud forcing on the following summer sea-ice distribution could be another sea-ice long-term memory mechanism in the Antarctic in addition to the phenomenon of sea-ice anomaly reemergence. The reemergence is caused by spring sea ice associated ocean heat anomalies that are retained at depth over summer and return to the surface as mixed layers deepen during the austral autumn, which induce sea-ice anomalies during the growth season. The long-term memory of reemergence is stored in the ocean, and it relates sea surface temperature anomalies from the previous melting season to sea-ice growth after the summer (Holland et al., 2013). The long-term memory of winter cloud forcing is stored in sea ice, in which winter ice anomaly can persist through seasons and result in summer sea-ice anomalies.

Although we have demonstrated that the cloud forcing in winter 2011 played a critical role in the sea-ice rebound in summer 2012, our sea-ice growth estimates do not include all forcing. Among all missing components, the ocean feedback could be significant in the Antarctic (Martinson & Iannuzzi, 1998). In future works, we will improve the analytical sea-ice growth model to evaluate the relative importance of winter cloud forcing and investigate the relationship between the interdecadal variability in clouds and sea ice in the Antarctic.

## References

- Bintanja, R., van Oldenborgh, G. J., Drijfhout, S. S., Wouters, B., & Katsman, C. A. (2013). Important role for ocean warming and increased ice-shelf melt in Antarctic sea-ice expansion. *Nature Geoscience*, 6(5), 376–379. <https://doi.org/10.1038/ngeo1767>
- Bosilovich, M. G., Robertson, F. R., & Chen, J. (2011). Global energy and water budgets in MERRA. *Journal of Climate*, 24(22), 5721–5739. <https://doi.org/10.1175/2011JCLI4175.1>
- Cavalieri, D. J., & Parkinson, C. L. (2008). Antarctic sea ice variability and trends, 1979–2006. *Journal of Geophysical Research*, 113, C07004. <https://doi.org/10.1029/2007JC004564>
- Clem, K. R., & Fogt, R. L. (2015). South Pacific circulation changes and their connection to the tropics and regional Antarctic warming in austral spring, 1979–2012. *Journal of Geophysical Research: Atmospheres*, 120, 2773–2792. <https://doi.org/10.1002/2014JD022940>
- Comiso, J. C., Meier, W. N., & Gersten, R. (2017). Variability and trends in the Arctic sea ice cover: Results from different techniques. *Journal of Geophysical Research: Oceans*, 122, 6883–6900. <https://doi.org/10.1002/2017JC012768>
- Comiso, J. C., & Nishio, F. (2008). Trends in the sea ice cover using enhanced and compatible AMSR-E, SSM/I, and SMMR data. *Journal of Geophysical Research*, 113, C02S07. <https://doi.org/10.1029/2007JC004257>
- Cuzzone, J., & Vavrus, S. (2011). The relationships between Arctic sea ice and cloud-related variables in the ERA-Interim reanalysis and CCSM3. *Environmental Research Letters*, 6, 014016. <https://doi.org/10.1088/1748-9326/6/1/014016>
- Dee, D. P., Uppala, S. M., Simmons, A. J., Berrisford, P., Poli, P., Kobayashi, S., et al. (2011). The ERA-Interim reanalysis: Configuration and performance of the data assimilation system. *Quarterly Journal of the Royal Meteorological Society*, 137(656), 553–597. <https://doi.org/10.1002/qj.828>
- Dolinar, E. K., Dong, X., & Xi, B. (2016). Evaluation and intercomparison of clouds, precipitation, and radiation budgets in recent reanalyses using satellite-surface observations. *Climate Dynamics*, 46(7–8), 2123–2144. <https://doi.org/10.1007/s00382-015-2693-z>
- Eisenman, I., Untersteiner, N., & Wettlaufer, J. S. (2007). On the reliability of simulated Arctic sea ice in global climate models. *Geophysical Research Letters*, 34, L10501. <https://doi.org/10.1029/2007GL029914>
- Fan, T., Deser, C., & Schneider, D. P. (2014). Recent Antarctic sea ice trends in the context of Southern Ocean surface climate variations since 1950. *Geophysical Research Letters*, 41, 2419–2426. <https://doi.org/10.1002/2014GL029239>

## Acknowledgments

We thank the NSIDC for providing the SIC and sea-ice motion data, at their website <http://nsidc.org/data/search/#sortKeys=score,,desc/facetFilters=%257B%257D/pageNumber=1/itemsPerPage=25>. The MERRA reanalysis data sets, including the data sets for cloud fraction, the surface net downward shortwave, and longwave flux under all and clear-sky conditions, geopotential height, vertical pressure velocity, wind, air temperature, and specific humidity were obtained from the Goddard Earth Sciences Data and Information Services Center (GES DISC) at the website <https://disc.gsfc.nasa.gov/datasets?keywords=merra&page=1>. The cloud fraction product from the ERA-Interim reanalysis was obtained from the ECMWF (<https://apps.ecmwf.int/datasets/data/interim-full-mode/levtype=pl/>). The APP-X climate data sets, including the cloud fraction and sea-ice thickness, were obtained from the National Centers for Environmental Information (NCEI) of National Oceanic and Atmospheric Administration NOAA (<https://www.ncdc.noaa.gov/cdr/atmospheric/extended-avhrr-polar-pathfinder-app-x>). The cloud fraction data from the ISCCP was provided at the website <https://www.ncei.noaa.gov/data/international-satellite-cloud-climate-project-iscsp-h-series-data/access/>. We thank three anonymous reviewers for their very beneficial comments, which helped in improving the manuscript significantly. This work was supported by the National Natural Science Foundation of China under grant 41406215 and the NSFC-Shandong Joint Fund for Marine Science Research Centers (U1606401). Yuan is supported by the US NSF grant PLR-1443444. LDEO contribution number is 8293.

- Fogt, R. L., Wovrosh, A. J., Langen, R. A., & Simmonds, I. (2012). The characteristic variability and connection to the underlying synoptic activity of the Amundsen-Bellinghshausen Seas Low. *Journal of Geophysical Research*, *117*, D07111. <https://doi.org/10.1029/2011JD017337>
- Francis, J. A., Chan, W., Leathers, D. J., Miller, J. R., & Veron, D. E. (2009). Winter Northern Hemisphere weather patterns remember summer Arctic sea-ice extent. *Geophysical Research Letters*, *36*, L07503. <https://doi.org/10.1029/2009GL037274>
- Gagné, M. È., Gillett, N. P., & Fyfe, J. C. (2015). Observed and simulated changes in Antarctic sea ice extent over the past 50 years. *Geophysical Research Letters*, *42*, 90–95. <https://doi.org/10.1002/2014GL062231>
- Graversen, R. G., Mauritsen, T., Drijfhout, S., Tjernström, M., & Mårtensson, S. (2011). Warm winds from the Pacific caused extensive Arctic sea-ice melt in summer 2007. *Climate Dynamics*, *36*(11–12), 2103–2112. <https://doi.org/10.1007/s00382-010-0809-z>
- Hobbs, W. R., Massom, R., Stammerjohn, S., Reid, P., Williams, G., & Meier, W. (2016). A review of recent changes in Southern Ocean sea ice, their drivers and forcings. *Global & Planetary Change*, *143*(C), 228–250. <https://doi.org/10.1016/j.gloplacha.2016.06.008>
- Holland, M. M., Blanchard-Wrigglesworth, E., Kay, J., & Vavrus, S. (2013). Initial-value predictability of Antarctic sea ice in the Community Climate System Model 3. *Geophysical Research Letters*, *40*, 2121–2124. <https://doi.org/10.1002/grl.50410>
- Holland, P. R. (2014). The seasonality of Antarctic sea ice trends. *Geophysical Research Letters*, *41*, 4230–4237. <https://doi.org/10.1002/2014GL060172>
- Holland, P. R., Bruneau, N., Enright, C., Losch, M., Kurtz, N. T., & Kwok, R. (2014). Modeled trends in Antarctic sea ice thickness. *Journal of Climate*, *27*(10), 3784–3801. <https://doi.org/10.1175/JCLI-D-13-00301.1>
- Holland, P. R., & Kwok, R. (2012). Wind-driven trends in Antarctic sea-ice drift. *Nature Geoscience*, *5*(12), 872–875. <https://doi.org/10.1038/ngeo1627>
- Huang, Y., Dong, X., Xi, B., Dolinar, E. K., & Stanfield, R. E. (2015). Quantifying the uncertainties of reanalyzed Arctic cloud and radiation properties using satellite-surface observations. *Climate Dynamics*, *30*(19), 8007–8029. <https://doi.org/10.1175/JCLI-D-16-0722.1>
- Jacobs, S. S., & Comiso, J. C. (1997). Climate variability in the Amundsen and Bellinghshausen seas. *Journal of Climate*, *10*(4), 697–709. [https://doi.org/10.1175/1520-0442\(1997\)010<0697:CVITAA>2.0.CO;2](https://doi.org/10.1175/1520-0442(1997)010<0697:CVITAA>2.0.CO;2)
- Jing, W., & Lin, S. (2017). Comparison and Evaluation of Different MODIS Aerosol Optical Depth Products Over the Beijing-Tianjin-Hebei Region in China. *IEEE Journal of Selected Topics in Applied Earth Observations & Remote Sensing*, *10*(3), 835–844. <https://doi.org/10.1109/JSTARS.2016.2595624>
- Kapsch, M. L., Graversen, R. G., & Tjernström, M. (2013). Springtime atmospheric energy transport and the control of Arctic summer sea-ice extent. *Nature Climate Change*, *3*(8), 744–748. <https://doi.org/10.1038/nclimate1884>
- Katlein, C., Hendricks, S., & Key, J. (2017). Brief communication: Increasing shortwave absorption over the Arctic Ocean is not balanced by trends in the Antarctic. *The Cryosphere*, *11*(5), 2111. <https://doi.org/10.5194/tc-11-2111-2017>
- Kauker, F., Kaminski, T., Karcher, M., Giering, R., Gerdes, R., & Voßbeck, M. (2009). Adjoint analysis of the 2007 all time Arctic sea-ice minimum. *Geophysical Research Letters*, *36*, L03707. <https://doi.org/10.1029/2008GL036323>
- Key, J. R. (2016). The AVHRR polar pathfinder climate data records. *Remote Sensing*, *8*(3), 167. <https://doi.org/10.3390/rs8030167>
- Lee, S., Gong, T., Feldstein, S. B., Screen, J. A., & Simmonds, I. (2017). Revisiting the cause of the 1989–2009 Arctic surface warming using the surface energy budget: Downward infrared radiation dominates the surface fluxes. *Geophysical Research Letters*, *44*, 10,654–10,661. <https://doi.org/10.1002/2017GL075375>
- Lefebvre, W., Goosse, H., Timmermann, R., & Fichefet, T. (2004). Influence of the Southern Annular Mode on the sea ice-ocean system. *Journal of Geophysical Research*, *109*, C09005. <https://doi.org/10.1029/2004JC002403>
- Lin, S., Mi, X., Jing, W., Jian, W., Tian, X., Yu, H., & Ping, G. (2016). A cloud detection algorithm-generating method for remote sensing data at visible to short-wave infrared wavelengths. *Isprs Journal of Photogrammetry & Remote Sensing*, *124*, 70–88. <https://doi.org/10.1016/j.isprs.2016.12.005>
- Liu, J., & Curry, J. A. (2010). Accelerated warming of the Southern Ocean and its impacts on the hydrological cycle and sea ice. *Proceedings of the National Academy of Sciences of the United States of America*, *107*(34), 14,987–14,992. <https://doi.org/10.1073/pnas.1003336107>
- Liu, N., Lin, L., Kong, B., Wang, Y., Zhang, Z., & Chen, H. (2016). Association between Arctic autumn sea ice concentration and early winter precipitation in China. *Acta Oceanologica Sinica*, *35*(5), 73–78.
- Liu, N., Lin, L., Wang, Y., Kong, B., Zhang, Z., & Chen, H. (2016). Arctic autumn sea ice decline and Asian winter temperature anomaly. *Acta Oceanologica Sinica*, *35*(7), 36–41. <https://doi.org/10.1007/s13131-016-0911-0>
- Liu, Y., & Key, J. R. (2014). Less winter cloud aids summer 2013 Arctic sea ice return from 2012 minimum. *Environmental Research Letters*, *9*(4). <https://doi.org/10.1088/1748-9326/9/4/044002>
- Liu, Y., Key, J. R., Liu, Z., Wang, X., & Vavrus, S. J. (2012). A cloudier Arctic expected with diminishing sea ice. *Geophysical Research Letters*, *39*, L05705. <https://doi.org/10.1029/2012GL051251>
- Liu, Y. H., Key, J. R., & Wang, X. J. (2009). Influence of changes in sea ice concentration and cloud cover on recent Arctic surface temperature trends. *Geophysical Research Letters*, *36*, L20710. <https://doi.org/10.1029/2009GL040708>
- Luo, B., Luo, D., Wu, L., Zhong, L., & Simmonds, I. (2017). Atmospheric circulation patterns which promote winter Arctic sea ice decline. *Environmental Research Letters*, *12*, 1–13. <https://doi.org/10.1088/1748-9326/aa69d0>
- Manabe, S., Stouffer, R. J., Spelman, M. J., & Bryan, K. (1991). Transient responses of a coupled ocean-atmosphere model to gradual changes of atmospheric CO<sub>2</sub>. Part I. Annual mean response. *Journal of Climate*, *4*(5), 105–126. [https://doi.org/10.1175/1520-0442\(1992\)005<0105:TROACO>2.0.CO;2](https://doi.org/10.1175/1520-0442(1992)005<0105:TROACO>2.0.CO;2)
- Martinson, D. G., & Iannuzzi, R. A. (1998). Antarctic ocean-ice interaction: Implications from ocean bulk property distributions in the Weddell Gyre. In M. Jeffries (Ed.), *Antarctic research series, Antarctic sea ice: Physical processes* (pp. 243–271). interactions and variability. <https://doi.org/10.1029/AR074p0243>
- Massonnet, F., Mathiot, P., Fichefet, T., Goosse, H., Beatty, C. K., Vancoppenolle, M., & Laverne, T. (2013). A model reconstruction of the Antarctic sea ice thickness and volume changes over 1980–2008 using data assimilation. *Ocean Modelling*, *64*(3), 67–75. <https://doi.org/10.1016/j.ocemod.2013.01.003>
- Maykut, G. A., Grenfell, T. C., & Weeks, W. F. (1992). On estimating spatial and temporal variations in the properties of ice in the polar oceans. *Journal of Marine Systems*, *3*(1–2), 41–72. [https://doi.org/10.1016/0924-7963\(92\)90030-C](https://doi.org/10.1016/0924-7963(92)90030-C)
- Meehl, G. A., Arblaster, J. M., Bitz, C. M., Chung, C. T. Y., & Teng, H. (2016). Antarctic sea-ice expansion between 2000 and 2014 driven by tropical Pacific decadal climate variability. *Nature Geoscience*, *9*(8), 590–595. <https://doi.org/10.1038/ngeo2751>
- Mei, L., Xue, Y., Xu, H., Jie, G., Li, Y., Wang, Y., et al., (2012). Validation and analysis of aerosol optical thickness retrieval over land. *International Journal of Remote Sensing*, *33*(3), 781–803. <https://doi.org/10.1080/01431161.2011.577831>
- Nussbaumer, E. A., & Pinker, R. T. (2012). The role of shortwave radiation in the 2007 Arctic sea ice anomaly. *Geophysical Research Letters*, *39*, L15808. <https://doi.org/10.1029/2012GL052415>

- Palm, S. P., Strey, S. T., Spinhirne, J., & Markus, T. (2010). Influence of Arctic sea ice extent on polar cloud fraction and vertical structure and implications for regional climate. *Journal of Geophysical Research*, *115*, D21209. <https://doi.org/10.1029/2010JD013900>
- Parkinson, C. L., & Cavalieri, D. J. (2008). Arctic sea ice variability and trends, 1979–2006. *Journal of Geophysical Research*, *113*, C07003. <https://doi.org/10.1029/2007JC004558>
- Parkinson, C. L., & Cavalieri, D. J. (2012). Antarctic sea ice variability and trends, 1979–2010. *The Cryosphere*, *6*(4), 871–880. <https://doi.org/10.5194/tc-6-871-2012>
- Parkinson, C. L., & Washington, W. M. (1979). A large-scale numerical model of sea ice. *Journal of Geophysical Research*, *84*(C1), 311–337. <https://doi.org/10.1029/JC084iC01p00311>
- Pezza, A. B., Rashid, H. A., & Simmonds, I. (2012). Climate links and recent extremes in Antarctic sea ice, high-latitude cyclones, Southern Annular Mode and ENSO. *Climate Dynamics*, *38*(1–2), 57–73. <https://doi.org/10.1007/s00382-011-1044-y>
- Polvani, L. M., & Smith, K. L. (2013). Can natural variability explain observed Antarctic sea ice trends? New modeling evidence from CMIP5. *Geophysical Research Letters*, *40*, 3195–3199. <https://doi.org/10.1002/grl.50578>
- Raphael, M. N., Marshall, G. J., Turner, J., Fogt, R. L., Schneider, D., Dixon, D. A., et al. (2016). The Amundsen Sea Low: Variability, change, and impact on Antarctic climate. *Bulletin of the American Meteorological Society*, *97*(1), 197–210. <https://doi.org/10.1175/BAMS-D-14-00018.1>
- Rignot, E., Jacobs, S., Mouginot, J., & Scheuchl, B. (2013). Ice-shelf melting around Antarctica. *Science*, *341*(6143), 266–270. <https://doi.org/10.1126/science.1235798>
- Rosenfeld, D., Sherwood, S., Wood, R., & Donner, L. (2014). Climate effects of aerosol-cloud interactions. *Science*, *343*(6169), 379–380. <https://doi.org/10.1126/science.1247490>
- Schweiger, A. J., Zhang, J., Lindsay, R. W., & Steele, M. (2008). Did unusually sunny skies help drive the record sea ice minimum of 2007? *Geophysical Research Letters*, *35*, L15053. <https://doi.org/10.1029/2008GL033463>
- Screen, J. A., & Simmonds, I. (2012). Declining summer snowfall in the Arctic: Causes, impacts and feedbacks. *Climate Dynamics*, *38*(11–12), 2243–2256. <https://doi.org/10.1007/s00382-011-1105-2>
- Simmonds, I. (2015). Comparing and contrasting the behaviour of Arctic and Antarctic sea ice over the 35 year period 1979–2013. *Annals of Glaciology*, *56*(69), 18–28. <https://doi.org/10.3189/2015AoG69A909>
- Stammerjohn, S., Massom, R., Rind, D., & Martinson, D. (2012). Regions of rapid sea ice change: An inter-hemispheric seasonal comparison. *Geophysical Research Letters*, *39*, L06501. <https://doi.org/10.1029/2012GL050874>
- Stroeve, J. C., Serreze, M. C., Holland, M. M., Kay, J. E., Malanik, J., & Barrett, A. P. (2012). The Arctic's rapidly shrinking sea ice cover: A research synthesis. *Climatic Change*, *110*(3–4), 1005–1027. <https://doi.org/10.1007/s10584-011-0101-1>
- Sun, L., Wei, J., Bilal, M., Tian, X., Jia, C., Guo, Y., & Mi, X. (2015). Aerosol Optical Depth Retrieval over Bright Areas Using Landsat 8 OLI Images. *Remote Sensing*, *8*(1), 23. <https://doi.org/10.3390/rs8010023>
- Svensson, G., & Karlsson, J. (2011). On the Arctic wintertime climate in global climate models. *Journal of Climate*, *24*(22), 5757–5771. <https://doi.org/10.1175/2011JCLI4012.1>
- Tamura, T., Ohshima, K. I., Fraser, A. D., & Williams, G. D. (2016). Sea ice production variability in Antarctic coastal polynyas. *Journal of Geophysical Research: Oceans*, *121*, 2967–2979. <https://doi.org/10.1002/2015jc011537>
- Tamura, T., Ohshima, K. I., & Nihashi, S. (2008). Mapping of sea ice production for Antarctic coastal polynyas. *Geophysical Research Letters*, *35*, L07606. <https://doi.org/10.1029/2007GL032903>
- Turner, J., Hosking, J. S., Marshall, G. J., Phillips, T., & Bracegirdle, T. J. (2016). Antarctic sea ice increase consistent with intrinsic variability of the Amundsen Sea Low. *Climate Dynamics*, *46*(7–8), 2391–2402. <https://doi.org/10.1007/s00382-015-2708-9>
- Wang, Q., Sun, L., Wei, J., Yang, Y., Li, R., Liu, Q., & Chen, L. (2017). Validation and Accuracy Analysis of Global MODIS Aerosol Products over Land. *Atmosphere*, *8*(8), 155. <https://doi.org/10.3390/atmos8080155>
- Wang, X., & Key, J. R. (2003). Recent trends in Arctic surface, cloud, and radiation properties from space. *Science*, *299*(5613), 1725–1728. <https://doi.org/10.1126/science.1078065>
- Wang, X., & Key, J. R. (2005a). Arctic surface, cloud, and radiation properties based on the AVHRR polar pathfinder dataset Part I: Spatial and Temporal Characteristics. *Journal of Climate*, *18*(14), 2558–2574. <https://doi.org/10.1175/JCLI3438.1>
- Wang, X., & Key, J. R. (2005b). Arctic surface, cloud, and radiation properties based on the AVHRR polar pathfinder dataset Part II: Recent Trends. *Journal of Climate*, *18*(14), 2575–2593. <https://doi.org/10.1175/JCLI3439.1>
- Wang, X., Key, J. R., & Liu, Y. (2010). A thermodynamic model for estimating sea and lake ice thickness with optical satellite data. *Journal of Geophysical Research*, *115*, C12035. <https://doi.org/10.1029/2009JC005857>
- Wang, Y., Bi, H., Huang, H., Liu, Y., Liu, Y., Liang, X., et al. (2018). Satellite-observed trends in the Arctic sea ice concentration for the period 1979–2016. *Journal of Oceanology and Limnology*, *37*(1), 18–37. <https://doi.org/10.1007/s00343-019-7284-0>
- Wu, T., Fan, M., Tao, J., Su, L., Wang, P., Liu, D., et al. (2017). Aerosol Optical Properties over China from RAMS-CMAQ Model Compared with CALIOP Observations. *Atmosphere*, *8*(10), 201. <https://doi.org/10.3390/atmos8100201>
- Yuan, X., & Li, C. (2008). Climate modes in southern high latitudes and their impacts on Antarctic sea ice. *Journal of Geophysical Research*, *113*, C06S91. <https://doi.org/10.1029/2006JC004067>
- Yuan, X., & Martinson, D. G. (2001). The Antarctic dipole and its predictability. *Geophysical Research Letters*, *28*(18), 3609–3612. <https://doi.org/10.1029/2001GL012969>
- Yuan, X., & Yonekura, E. (2011). Decadal variability in the Southern Hemisphere. *Journal of Geophysical Research*, *116*, D19115. <https://doi.org/10.1029/2011JD015673>
- Zhai, M., Li, X., Hui, F., Cheng, X., Heil, P., Zhao, T., et al. (2017). Sea ice conditions in the Adélie depression during besetment of the Chinese icebreaker RV Xuelong. *Annals of Glaciology*, *56*(69), 160–166. <https://doi.org/10.3189/2015AoG69A007>
- Zhang, H., Cao, Y., Zhang, Y., & Terzija, V. (2018). Quantitative synergy assessment of regional wind-solar energy resources based on MERRA reanalysis data. *Applied Energy*, *216*(C), 172–182. <https://doi.org/10.1016/j.apenergy.2018.02.094>
- Zhang, J. (2008). Increasing Antarctic sea ice under warming atmospheric and oceanic conditions. *Journal of Climate*, *20*(11), 2515–2529. <https://doi.org/10.1175/JCLI4136.1>
- Zhang, J. (2014). Modeling the impact of wind intensification on Antarctic sea ice volume. *Journal of Climate*, *27*(1), 202–214. <https://doi.org/10.1175/JCLI-D-12-00139.1>